Plasmonics (2014) 9:765–772
DOI 10.1007/s11468-013-9657-0

Gold Nanoring Arrays for Near Infrared Plasmonic Biosensing

Mana Toma · Kyunghee Cho · Jennifer B. Wood · Robert M. Corn

Received: 25 November 2013 / Accepted: 2 December 2013 / Published online: 22 December 2013

Abstract Gold nanoring array surfaces that exhibit strong localized surface plasmon resonances (LSPR) at near infrared (NIR) wavelengths from 1.1 to 1.6 μm were used as highly sensitive real-time refractive index biosensors. Arrays of gold nanorings with tunable diameter, width, and spacing were created by the nanoscale electrodeposition of gold nanorings onto lithographically patterned nanohole array conductive surfaces over large areas (square centimeters). The bulk refractive index sensitivity of the gold nanoring arrays was determined to be up to 3,780 cm^{-1}/refractive index unit by monitoring shifts in the LSPR peak by FT-NIR transmittance spectroscopy measurements. As a first application, the surface polymerization reaction of dopamine to form polydopamine thin films on the nanoring sensor surface from aqueous solution was monitored with the real-time LSPR peak shift measurements. To demonstrate the utility of the gold nanoring arrays for LSPR biosensing, the hybridization adsorption of DNA-functionalized gold nanoparticles onto complementary DNA-functionalized gold nanoring arrays was monitored. The adsorption of DNA-modified gold nanoparticles onto nanoring arrays modified with mixed DNA monolayers that contained only 0.5 % complementary DNA was also detected; this relative surface coverage corresponds to the detection of DNA by hybridization adsorption from a 50 pM solution.

Keywords Gold nanorings · Periodic nanoring arrays · Localized surface plasmon resonance · DNA biosensor · Near infrared

M. Toma · K. Cho · J. B. Wood · R. M. Corn (✉)
Department of Chemistry, University of California—Irvine, Irvine, CA 92697, USA
e-mail: rcorn@uci.edu

Introduction

Surface plasmon resonance (SPR) measurement based on the excitation of propagating surface plasmon polaritons on planar metallic surfaces is a well-established and sensitive biosensing method for the detection of surface bioaffinity interactions and the quantitative analysis of target proteins and nucleic acids with applications to the fields of medical diagnostics, food safety, and environmental monitoring [1, 2]. Localized surface plasmon resonance (LSPR) measurement based on the excitation of localized surface plasmons on nanostructured metal surfaces is an alternative biosensing method that is easily incorporated into a simple absorption spectroscopy format; LSPR measurements have been suggested as a potentially higher sensitivity detection method than SPR [3, 4].

In a typical LSPR biosensor, the binding of target biomolecules onto metal nanostructured surfaces is detected as a shift in resonant wavelength in the absorption spectrum. The plasmonic properties which determine the sensitivity of LSPR biosensors highly depend on the geometry of the metal nanostructures [4, 5]; arrays of nanoparticles [6, 7], nanocubes [8, 9], nanopyramids [10], nanodisks [11, 12], nanorods [13–15], and nanorings [16–18] have all been employed as LSPR biosensor surfaces. Metallic nanoring arrays have emerged as one of the most promising nanostructured surfaces due to their unique plasmonic properties and potential for enhanced refractive index sensitivity [16, 19]. Previous studies have revealed that the resonant wavelength and refractive index sensitivity of the nanoring LSPR biosensors depend critically on the spacing, diameter, and width of the nanorings [16, 19, 20]. A variety of sequential methods for fabricating metallic nanorings such as electron beam lithography [18] and nanoimprint lithography [19] have been explored. These methods offer excellent geometric control of the nanoring array dimensions but are limited in the total area that the

nanostructures can be created. Methods that employ colloidal or nanosphere lithography have been used to create nanoring arrays over larger surface areas, but the geometric control of the diameter and width of the nanorings has been limited with these fabrication methods [16, 17, 21].

Recently, we have developed a new method for fabricating metallic nanoring arrays over large surface areas that uses a combination of colloidal lithography and lithographically patterned nanoscale electrodeposition (LPNE), as shown schematically in Fig. 1 [22]. This new method can be used to create periodically ordered gold nanoring (Au nanoring) arrays over large surface areas with excellent control of the nanoring diameter, width, and spacing [22]. The Au nanoring arrays created by this process exhibit strong and tunable LSPR absorption bands at the NIR wavelengths from 1.0 to 2.5 μm with narrow bandwidths that are potentially useful for refractive index biosensing measurements.

In this paper, the refractive index sensitivity of a series of Au nanoring arrays with various nanoring dimensions created by this LPNE process is reported. Real-time Fourier transform near infrared (FT-NIR) transmittance measurements were used to determine a bulk refractive index sensitivity of 3,780 cm^{-1}/refractive index unit (RIU) for LSPR measurements of nanoring arrays. A series of real-time, in situ FT-NIR transmittance measurements were then used to monitor the polymerization of dopamine to form a multilayer film of polydopamine on the nanoring sensor surface. In a third LSPR experiment, the hybridization adsorption of DNA-functionalized gold nanoparticles (AuNPs) onto Au nanoring array surfaces modified with complementary DNA was characterized. The sensitivity of DNA detection with these nanoring arrays was estimated by monitoring the hybridization adsorption of DNA-functionalized AuNPs onto mixed DNA monolayers that only contain a small percentage of complementary DNA on the Au nanorings. The quantitative analysis of LSPR shifts induced by adsorption of DNA-modified AuNPs onto the nanorings revealed that the lowest detectable surface coverage of complementary DNA on Au nanoring arrays is 0.5 % of a monolayer, which corresponds to the relative surface coverage of DNA that would be created by exposure to a 50 pM DNA solution.

Materials and Methods

Materials

Carboxylate-coated polystyrene (PS) beads solutions (2.6 % *w*/*v*, 1 μm or 0.75 μm diameter) were obtained from Polysciences. Shipley S1808 photoresist, Thinner P, and MF-319 developer were purchased from Microchem. Clean Earth Chemicals 24-K gold plating solution was obtained from Grobet USA. 11-amino-1-undecanethiol hydrochloride (MUAM) was purchased from Dojindo (Japan). 1-ethyl-3-(3-(dimethylamino)propyl)carbodiimide hydrochloride (EDC) and N-hydroxysulfosuccinimide (Sulfo-NHS) were obtained from Thermo Scientific. Poly(L-glutamic acid) sodium salt (pGlu) and dopamine hydrochloride were obtained from Sigma. Three single-stranded DNA (ssDNA) sequences were purchased from Integrated DNA Technologies. The sequences are denoted A, Ac, and B: A=5′-NH_2-$(CH_2)_{12}$-CGAAATCCAGACACATAAGCACGAACCGAA-3′, Ac=5′-TTCGGTTCGTGCTTATGTGTCTGGATTTCG-$(CH_2)_{12}$-SH-3′, and B=5′-NH_2-$(CH_2)_{12}$-$(T)_{30}$-3′.
All the chemicals were used as received.

Preparation of DNA-modified Gold Nanoparticles

AuNPs with a diameter of ~13 nm were synthesized by citrate reduction based on the Turkevich Method [23]. Briefly, $HAuCl_4$ (0.0223 g, 0.0656 mmol) was dissolved in 100 mL water. Sodium citrate dihydrate (0.0533 g, 0.1812 mmol, in 5 mL water) was then injected to the boiling solution. After a color change (from blue to red) was observed, the reaction solution was continued to boil for 10 min. AuNPs solution (1 mL) was filtered (0.22 μm) prior to the addition of 1 mM thiol-terminated ssDNA (5 μL, in phosphate-buffered saline (PBS) buffer). After the mixture was kept at 37 °C for 24 h, 500 μL of PBS buffer was added to the solution. The solution was kept at 37 °C for another 24 h to complete the ligand exchange reaction. Two centrifugation cycles (13,000 rpm, 15 min) were applied to remove the excess ssDNA in the solution, followed by removal of supernatant and resuspension in PBS buffer. The concentration of AuNPs was measured by UV–vis spectroscopy with an extinction coefficient of 2.7×10^8 M^{-1} cm^{-1} at λ_{max}=520 nm and adjusted to approximately 2.5 nM.

Preparation of Au Nanoring Arrays

The detailed process for lithographically patterned electrodeposition of Au nanoring arrays has been described in our previous work [22]. First, a solution containing PS beads (5 % *w*/*v* in mixture of water and MeOH with mix ratio of 1:3) was spin-coated on cleaned BK7 glass and close-packed colloidal monolayer was formed as the solvent dried, shown in Fig. 1a. The size of PS beads was reduced by O_2 plasma treatment (South Bay Technologies) at 200 mTorr and 50 W (Figs. 1b). The etching time was set between 3.5 and 6 min to control the size of PS beads. The sacrificial electrode with nanohole arrays was created by deposition of a 70 nm thick Ni layer on top of the shrunk PS beads monolayer by a thermal evaporator (DV-502A, Denton Vacuum), followed by removal of PS beads with ultra-sonication in toluene for 10 min (Figs. 1c). Shipley S1808 photoresist (diluted to 1:1 with Thinner P) was spin-coated on top of the substrate in order to protect the surface of the sacrificial Ni layer. After

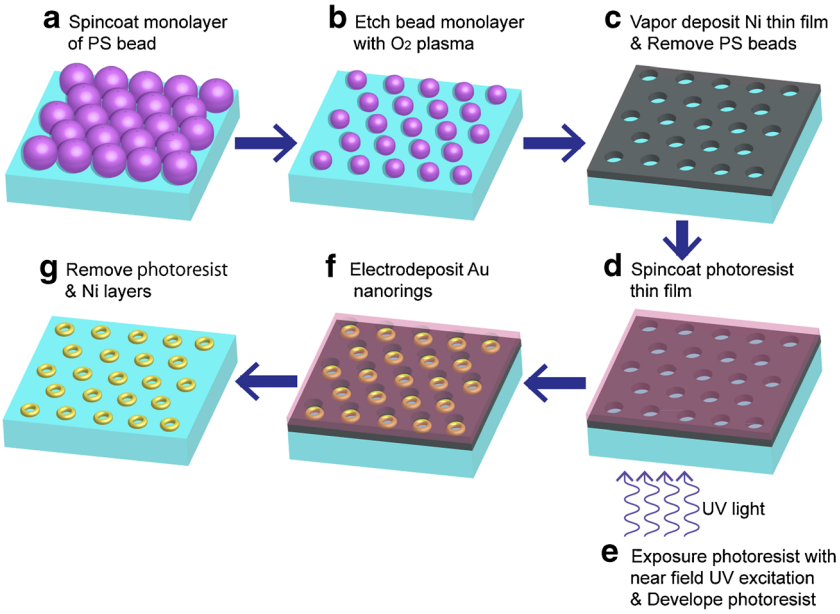

Fig. 1 **a**-**f** Fabrication process of lithographically patterned electrodeposition of Au nanoring arrays

spin-coating photoresist, the substrate was baked in an oven for 15 min at 90 °C. Subsequently, the photoresist was exposed to the UV light from the backside with an exposure dose of 30 mW/cm^2 (see Figs. 1d-e) and developed by MF-319 developer. Au nanorings were formed inside the Ni nanohole arrays by electrodeposition of Au using a potentiostat (PGSTAT12, Metrohm), shown in Fig. 1f. The potential and plating time were set to −0.85 V and 450 to 650 s, respectively. The width of the ring was controlled by the plating time. Finally, the sacrificial Ni layer was removed by immersing the substrate in 0.8 M nitric acid for 10 min (Fig. 1g). Before use, the substrates were annealed in a furnace for 45 min at 400 °C in order to smooth the surface of Au nanorings.

DNA Attachment onto Au Nanorings

ssDNA was attached onto the surface of Au nanorings by using pGlu attachment chemistry as described in our previous work [24]. Briefly, MUAM monolayer was formed on the Au nanorings by immersing the substrate in a 1 mM MUAM solution in ethanol overnight. The substrate was rinsed with ethanol followed by water and dried under nitrogen stream. The pGlu layer was formed by exposing the substrate to a 2 mg/ml pGlu solution in PBS for 1 h. Amino-terminated ssDNA was immobilized to pGlu monolayer by exposing the substrate to 250 μM DNA in PBS containing 75 mM EDC and 15 mM Sulfo-NHS for 5 h. The substrate was then rinsed with water and dried under nitrogen stream after pGlu attachment and DNA immobilization.

FT-NIR Measurements

Near IR absorption spectra were taken by a Mattson RS-1 FT-IR spectrometer. Spectra in the near IR region (3,000–12,000 cm^{-1}) were collected with 100 scans and 4 cm^{-1} resolution. For the in situ measurement, a flow cell with a volume of 30 μl was attached to the substrate and the sample solution was flowed over the sensor surface by using a peristaltic pump.

SEM Observation

The shape and density of Au nanoring arrays were characterized by SEM (Magellan400 XHR SEM or Phillips XL-30 FEG SEM). The image analysis was carried out by using ImageJ (US National Institutes of Health, http://imagej.nih.gov/ij/) and Mathematica to characterize the nanoring dimensions [22].

Results and Discussions

Characterization of Au Nanoring Arrays

A set of Au nanoring arrays were prepared, and their plasmonic properties were investigated. Figure 2a is a typical photograph of an Au nanoring array on a glass substrate which shows that the Au nanoring arrays uniformly covered the surface of glass slides with the dimension of 2.5 × 2.5 cm^2. The SEM image shown in Fig. 2b revealed that the Au nanoring arrays consisted of multiple domains of two-dimensional hexagonal close-packed crystalline Au nanorings. The size of a single domain was approximately 10 to 30 μm. Defects of the structure such as merged rings, vacancies, and disordered structures were sometimes observed at the border of the domains. The inserted picture in Fig. 2b is the enlarged image of the single domain of the Au

nanoring array. Figure 2c shows a schematic of the Au nanoring arrays. In the following, we define the structure of the Au nanoring arrays by the distance between the centers of the neighboring nanoring L, the diameter d, and the width w of the ring. The distance L is controlled by the size of the PS beads. The diameter is determined by the etching time of PS beads. The width and height can be varied by the plating time of Au.

The plasmonic properties of Au nanoring arrays with various diameter d and width w were characterized by FT-NIR spectroscopy. Figure 3 shows a set of near IR transmission absorption spectra of five Au nanoring arrays taken in air. The inserted pictures in the graph show typical SEM images of the nanorings. The absorption spectrum of sample E exhibited one strong absorption peak at 6,000 cm^{-1} and one weak absorption peak at 9,500 cm^{-1} associated with bonding mode and antibonding mode, respectively, in agreement with previous studies [18, 20]. In this paper, we have used the strong absorption peak of the bonding mode for the refractive index sensing. The prepared samples exhibited strong absorption peaks in the wide wavenumber range from 6,000 to 9,000 cm^{-1} with similar bandwidths. This wavenumber range corresponds to a wavelength range from 1.6 to 1.1 μm. The mean diameter and width of each sample were obtained from the average of over 100 nanorings in SEM pictures and were summarized in Table 1. The mean diameter of the nanoring was efficiently controlled over 100 nm by changing both plasma etching time and the size of PS beads. Samples A, B, and C were fabricated with 0.75 μm PS beads, and samples D and E were fabricated with 1 μm PS beads. The resonance absorption maximum shifted to higher wavenumber as the diameter of the nanoring was decreased. This trend agrees with theoretical and experimental results in previous studies [21, 22].

Bulk Refractive Index Sensitivity Measurements

The sensitivity of LSPRs of the Au nanoring arrays to changes in bulk refractive index was characterized by measuring shifts in the LSPR absorption peaks upon exposure of the Au nanoring arrays to solutions with different refractive indexes. The refractive index of the solution was changed by mixing water and ethanol with different mixture ratio (H_2O/EtOH=1:0, 3:1, 1:1, and 0:1). As the refractive indexes of water and ethanol exhibit a wavelength dependence, the refractive index of the sample solution at the resonance wavenumber was calculated from the Cauchy's constants of water and ethanol [25]. In order to eliminate the strong absorption peaks from the water and ethanol in the near IR region, a reference spectrum was taken with the sample solution without Au nanoring arrays. Figure 4a shows the changes in the absorption spectra of sample A when the sample

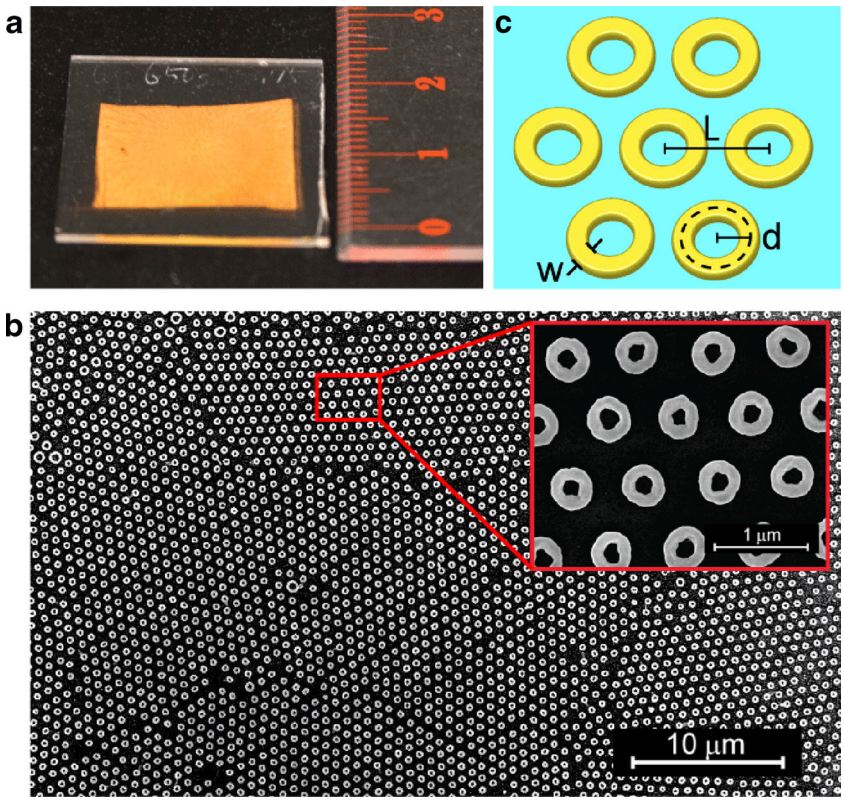

Fig. 2 **a** A representative photograph and **b** a SEM image of Au nanoring arrays on glass substrate. The inserted picture in SEM image is the enlarged image. **c** Schematic of the Au nanoring arrays with period L, diameter d, and width w

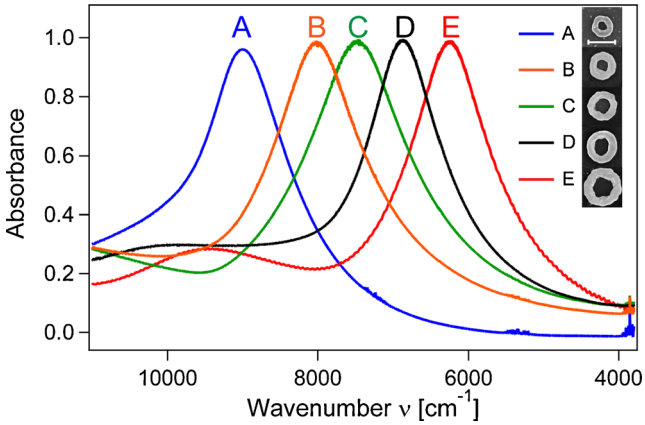

Fig. 3 Near IR absorption spectra of Au nanoring arrays in air. The inserted SEM images show the typical Au nanorings observed from each sample. The *scale bar* indicates 500 nm

was in contact with air (red curve), water (light blue curve), and ethanol (blue curve). The resonance wavenumber exhibited a large shift to lower wave numbers as the bulk refractive index increased without dramatic changes in the shape and the peak absorbance of the resonance curve. The peak wavenumber was determined by fitting the absorption spectra with Lorentzian function. Figure 4b plots the relative peak shift against the refractive index of the sample solution for the nanorings with various sizes shown in Fig. 3. All samples showed a linear dependence of the peak shift to bulk refractive indexes. The bulk refractive index sensitivity was obtained from the slope of the fitted curves. The sensitivities of sample A to E resulted in 3,780 to 2,700 cm^{-1}/RIU, respectively. As listed in Table 1, these sensitivities correspond to 805 to 1,020 nm/RIU in wavelength. The wavelength sensitivity agrees with the tendency that the sensitivity increases as resonance wavelength increases and relative width (w/d) decreases, as reported by Larsson et al. [16]. Our nanoring arrays exhibited enhanced sensitivities as compared to other metallic nanoring reported previously [16, 18]. Furthermore, these sensitivities were comparable to the state of the art refractive index LSPR sensors with more complicated nanostructures [26, 27].

Table 1 Dimensions, peak wavenumber, and bulk refractive index sensitivity of the samples shown in Fig. 3

	Distance L [nm]	Diameter d [nm]	Width w [nm]	Peak wavenumber ν_{max} [cm^{-1}]	Sensitivity [cm^{-1}/RIU (nm/RIU)]
A	750	146±8	124±6	8,995	−3,780 (805)
B	750	187±7	150±5	8,015	−3,447 (941)
C	750	204±−7	133±6	7,472	−3,238 (1,023)
D	1,000	213±10	150±6	6,867	−2,549 (960)
E	1,000	262±10	172±7	6,250	−2,413 (1,006)

Real-time Observation of Surface Polymerization of Dopamine

The polymerization process of dopamine at the surface of Au nanorings was monitored by real-time, in situ measurements of LSPR peak shifts. Polydopamine is a biomimetic adhesive polymer inspired by marine mussel foot proteins [28]. Polydopamine coating methods have attracted great attention due to the fact that they can be applied to any kind of surface by exposure to an alkaline dopamine solution. The coated thin polydopamine layer can serve as binding agent for biomolecules containing amino or thiol functional groups [29]. Characterization of polymerization process of dopamine is one of the key aspects requiring for the control of surface functionalization with polydopamine [30]. In this experiment, a sample solution containing 5 mg/ml dopamine in PBS buffer at pH 7.4 was used to create a polydopamine layer onto Au nanoring sensor surface as schematically illustrated in Fig. 5a.

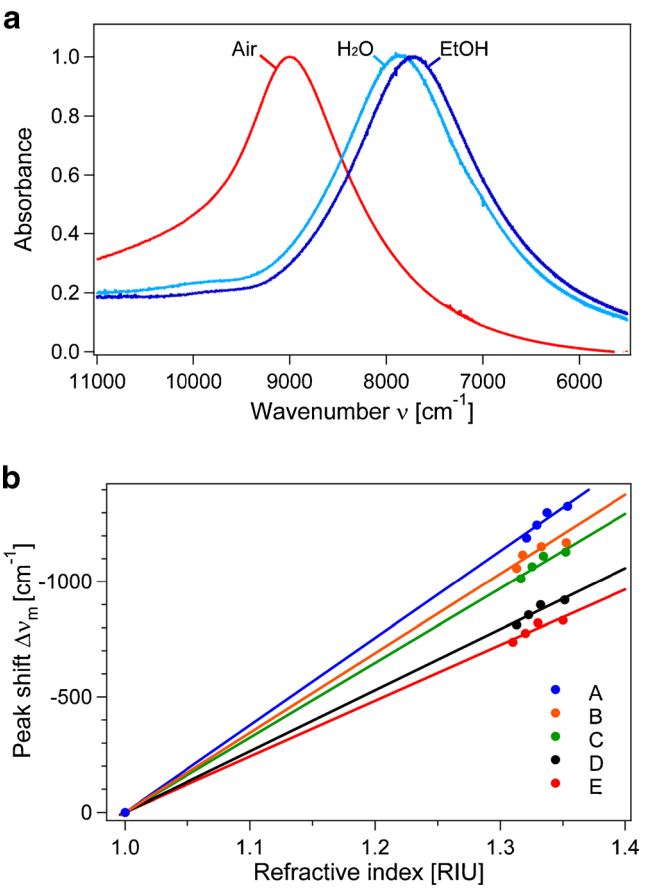

Fig. 4 **a** Absorption spectra of sample A in contact with air (*red curve*), water (*light blue curve*), and ethanol (blue curve). **b** Correlation curves between the peak shifts $\Delta\nu_m$ and bulk refractive indexes

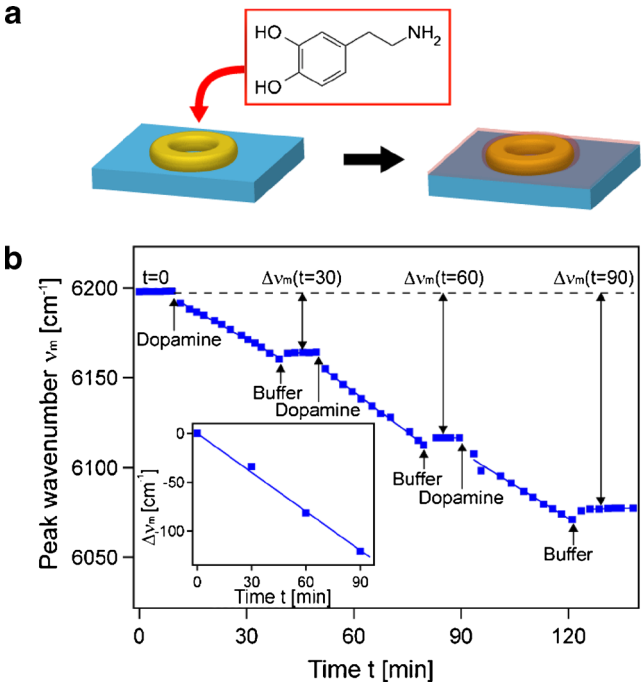

Fig. 5 **a** Schematic of adsorption of polydopamine multilayers onto Au nanorings. **b** Real-time in situ measurement of peak wavenumber ν_m upon polymerization of dopamine in a solution and its accumulation onto the Au nanoring arrays. The inserted graph shows the linear correlation between the peak shift $\Delta\nu_m$ and film growth time

The dopamine solution was flowed over the sensor surface for 30 min, and then the surface was rinsed with PBS for 10 min. This cycle was repeated three times. A series of FT-NIR absorption spectra were taken every 3 min, and the LSPR peak wavenumber ν_m was plotted as a function of time (see Fig. 5b). First, a baseline was obtained with the sensor surface in contact with PBS solution. When the dopamine solution was introduced, the peak wavenumber jumped to lower wavenumber, which is attributed to a bulk refractive index change around the Au nanorings. Subsequently, the peak wavenumber exhibited a constant shift to lower wavenumbers, indicating that dopamine molecules were polymerizing and adsorbing to form a polydopamine layer at the sensor surface. After the sensor surface was rinsed with PBS buffer, the peak wavenumber increased slightly and reached a plateau. This decrease in peak wavenumber is attributed to the increase of local refractive index by accumulation of polydopamine layers on the sensor surface. The inserted figure in Fig. 5b plots the peak shifts $\Delta\nu_m$ observed in PBS after multiple exposures to dopamine solutions. The peak shifts due to the polydopamine multilayer growth were increased linearly with time and were reached as large as 120 cm^{-1} after 90 min exposure. This observation agrees well with our recent SPR imaging study of the polymerization of dopamine on a flat Au thin films [30]. These results indicate that these near IR LSPR nanoring sensors are suitable for in situ monitoring of the adsorption of multilayer polymer films onto the sensor surfaces in real time.

Detection of DNA Hybridization Adsorption

In a third set of experiments, the DNA hybridization of AuNPs modified with ssDNA onto the Au nanoring arrays were detected with the near IR LSPR shift measurements [30, 31]. In this experiment, the surfaces of Au nanorings were functionalized with ssDNA by using pGlu attachment chemistry used previously [24]. The adsorption of AuNPs modified with complementary DNA (DNA–AuNPs) was monitored as the shift in resonance wavenumber as schematically illustrated in Fig. 6a. Figure 6b shows the FT-NIR spectra of the Au nanorings in PBS before and after binding of DNA–AuNPs to the DNA monolayer attached on the Au nanorings. The peak wavenumber exhibited a large shift of over 150 cm^{-1} after AuNPs adsorption.

A series of measurements of the hydridization adsorption of AuNPs onto partially complementary ssDNA monolayer was used to estimate the detection limit of ssDNA with LSPR on these nanoring arrays. In this experiment, Au nanoring arrays were functionalized with a mixture of two amino-terminated ssDNA (sequences A and B) at various A/B percentages of 100:0, 20:80, 10:90, 5:95, 1:99, 0.5:99.5, and 0:100. By assuming an equivalent surface reactivity of both ssDNA, the percentage of sequence A at the surface was controlled by the mixture ratio of A and B in the solution. In order to minimize the differences in sensitivity among samples, Au nanoring

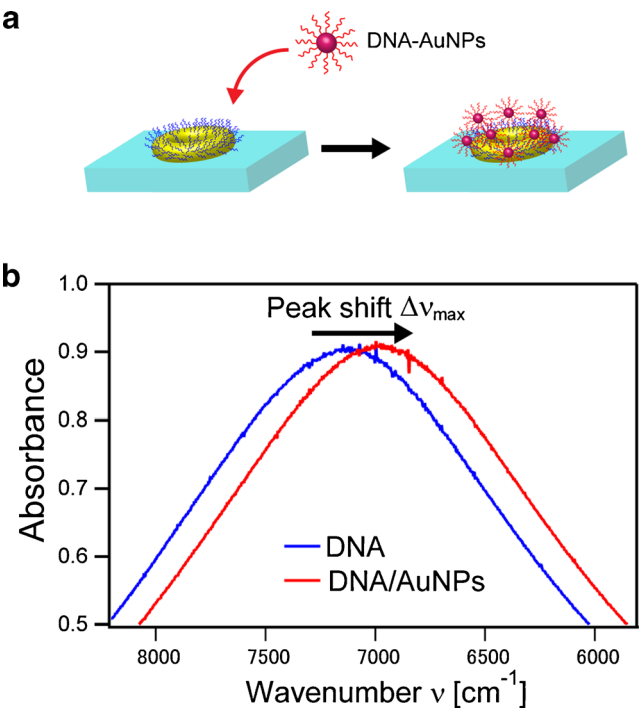

Fig. 6 Detection of DNA hybridization adsorption of AuNPs modified with ssDNA onto Au nanoring surface. **a** Schematic image of the sample. AuNPs functionalized with ssDNA (sequence Ac) bind to Au nanorings modified with a complementary DNA (sequence A) monolayer through DNA hybridization adsorption. **b** FT-NIR absorption spectra before (*blue curve*) and after (*red curve*) DNA–AuNPs adsorption

arrays with similar LSPR absorption peaks were used (8,180± 50 cm^{-1} in air). A solution containing 2.5 nM AuNPs modified with complementary DNA of sequence A (denoted Ac) was flowed over the sensor surface for 90 min and the shift in resonance wavenumber was monitored (see Fig. 7a). When the surface coverage of sequence A was 100 %, the resonance wavenumber of Au nanorings immediately shifted to lower wavenumber after the injection of AuNPs solution. Upon hybridization, the resonance wavenumber shifted by as much as 170 cm^{-1}. In contrast, for the surface modified entirely with noncomplementary DNA (100 % covered with sequence B), the shift in resonance wavenumber was negligible, indicating the high selectivity of DNA hybridization onto Au nanoring arrays and the lack nonspecific adsorption. Figure 7a also shows the adsorption curves observed for 5 and 0.5 % complementary ssDNA monolayer. A full set of steady state LSPR peak shifts as a function of percentage of sequence A (%A) is shown in Fig. 7b. The lowest %A surface coverage θ that could be measured was 0.5 %. This surface coverage θ corresponds to

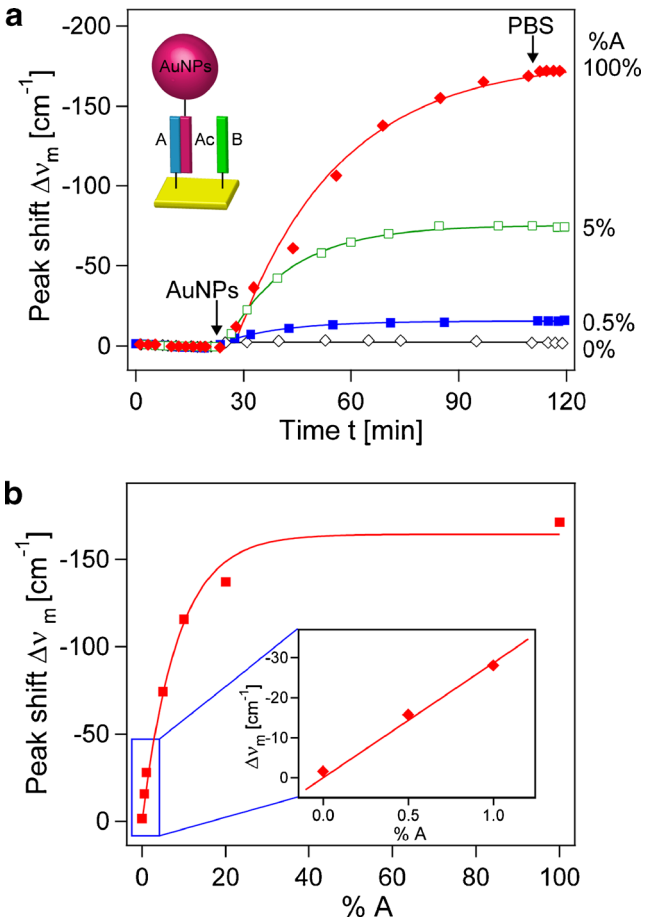

Fig. 7 **a** Real-time, in situ measurement of adsorption of DNA–AuNPs onto Au nanorings functionalized with complementary ssDNA with different relative surface coverage (%A=100, 5, 0.5, and 0 %). **b** Quantitative plot of peak shift $\Delta\nu_m$ as a function of %A. The peak shifts were obtained after the surface was rinsed with PBS buffer. The inserted figure is the enlarged plot where %A is below 1 %

that can be created by a DNA concentration C_{min} of 50 pM, assuming a Langmuir adsorption coefficient K_{ads} of 1.0×10^8 M^{-1} ($C_{min}=\theta/K_{ads}$) [30].

Conclusions

In this study, Au nanoring array surfaces exhibiting strong localized surface plasmon resonances at near infrared wavelengths were employed for refractive index biosensing by using FT-NIR transmittance spectroscopy. The Au nanoring arrays were fabricated by a simple bottom up process based on lithographically patterned nanoscale electrodeposition of Au nanorings, which enabled fabrication of Au nanoring arrays over large surface area with excellent control of the nanoring spacing, diameter, and width. The plasmonic absorption bands of Au nanoring arrays could be tuned from 1.1 to 1.6 μm in the NIR region by controlling the size and width of the nanorings. Real-time FT-NIR measurements were performed to detect changes in the bulk refractive index of solutions. The results revealed that the Au nanoring arrays exhibit a high bulk refractive index sensitivity up to 3,780 cm^{-1}/RIU, which is comparable to that of the state of the art of LSPR sensors with more complicated structures. Two examples of LSPR sensing with these Au nanoring arrays were performed: (1) the polymerization of dopamine to create polydopamine multilayers onto the nanoring sensor surface was monitored in real time, and (2) the hybridization adsorption of DNA-functionalized AuNPs onto Au nanoring arrays modified with complementary DNA was characterized. Using two component mixed DNA monolayers, relative surface coverages of complementary DNA as low as 0.5 % were detected, which corresponded to the detection of DNA by hybridization adsorption from a 50 pM solution. Our future work will include the fabrication of asymmetric nanoring structures such as split rings [32] and nanomushrooms [33] for further advanced sensitivities by using Fano type plasmon resonances.

Acknowledgments The authors thank the laboratory for electron and X-ray instrumentation (LEXI) for the use of the SEM and the plasma cleaner as well as Dr. J. Kim and Prof. R. M. Penner for the use of the furnace. This work was funded by NSF CHE-1057638.

References

1. Homola J (2008) Surface plasmon resonance sensors for detection of chemical and biological species. Chem Rev 108(2):462–493. doi:10.1021/cr068107d
2. Brolo AG (2012) Plasmonics for future biosensors. Nat Photonics 6(11):709–713. doi:10.1038/nphoton.2012.266
3. Mayer KM, Hafner JH (2011) Localized surface plasmon resonance sensors. Chem Rev 111(6):3828–3857. doi:10.1021/cr100313v

4. Anker JN, Hall WP, Lyandres O, Shah NC, Zhao J, Van Duyne RP (2008) Biosensing with plasmonic nanosensors. Nat Mater 7(6):442–453. doi:10.1038/nmat2162
5. Stewart ME, Anderton CR, Thompson LB, Maria J, Gray SK, Rogers JA, Nuzzo RG (2008) Nanostructured plasmonic sensors. Chem Rev 108(2):494–521. doi:10.1021/cr068126n
6. Willets KA, Van Duyne RP (2007) Localized surface plasmon resonance spectroscopy and sensing. Annu Rev Phys Chem 58:267–297. doi:10.1146/annurev.physchem.58.032806.104607
7. Haes AJ, Van Duyne RP (2002) A nanoscale optical biosensor: sensitivity and selectivity of an approach based on the localized surface plasmon resonance spectroscopy of triangular silver nanoparticles. J Am Chem Soc 124(35):10596–10604. doi:10.1021/ja020393x
8. Sherry LJ, Chang S-H, Schatz GC, Van Duyne RP, Wiley BJ, Xia Y (2005) Localized surface plasmon resonance spectroscopy of single silver nanocubes. Nano Lett 5(10):2034–2038. doi:10.1021/nl0515753
9. Mahmoud MA, Chamanzar M, Adibi A, El-Sayed MA (2012) Effect of the dielectric constant of the surrounding medium and the substrate on the surface plasmon resonance spectrum and sensitivity factors of highly symmetric systems: silver nanocubes. J Am Chem Soc 134(14):6434–6442. doi:10.1021/ja300901e
10. Kathryn MM, Feng H, Seunghyun L, Peter N, Jason HH (2010) A single molecule immunoassay by localized surface plasmon resonance. Nanotechnology 21(25):255503. doi:10.1088/0957-4484/21/25/255503
11. Lee S-W, Lee K-S, Ahn J, Lee J-J, Kim M-G, Shin Y-B (2011) Highly sensitive biosensing using arrays of plasmonic au nanodisks realized by nanoimprint lithography. ACS Nano 5(2):897–904. doi:10.1021/nn102041m
12. Jiang H, Li T, Ertorer E, Yang J, Sabarinathan J, Mittler S (2013) A biosensor based on periodic arrays of gold nanodisks under normal transmission. Sens Actuators, A 189:474–480. doi:10.1016/j.sna.2012.08.041
13. Marinakos SM, Chen SH, Chilkoti A (2007) Plasmonic detection of a model analyte in serum by a gold nanorod sensor. Anal Chem 79(14):5278–5283. doi:10.1021/ac0706527
14. Piliarik M, Sipova H, Kvasnicka P, Galler N, Krenn JR, Homola J (2012) High-resolution biosensor based on localized surface plasmons. Opt Express 20(1):672–680. doi:10.1364/OE.20.000672
15. Mayer KM, Lee S, Liao H, Rostro BC, Fuentes A, Scully PT, Nehl CL, Hafner JH (2008) A label-free immunoassay based upon localized surface plasmon resonance of gold nanorods. ACS Nano 2(4):687–692. doi:10.1021/nn7003734
16. Larsson EM, Alegret J, Käll M, Sutherland DS (2007) Sensing characteristics of NIR localized surface plasmon resonances in gold nanorings for application as ultrasensitive biosensors. Nano Lett 7(5):1256–1263. doi:10.1021/nl0701612
17. Chengjun H, Jian Y, Shuo W, Stakenborg T, Lagae L (2012) Gold nanoring as a sensitive plasmonic biosensor for on-chip DNA detection. Appl Phys Lett 100(17):173114. doi:10.1063/1.4707382
18. Tsai C-Y, Lu S-P, Lin J-W, Lee P-T (2011) High sensitivity plasmonic index sensor using slablike gold nanoring arrays. Appl Phys Lett 98(15):1530108. doi:10.1063/1.3579536
19. Kim S, Jung J-M, Choi D-G, Jung H-T, Yang S-M (2006) Patterned arrays of Au rings for localized surface plasmon resonance. Langmuir 22(17):7109–7112. doi:10.1021/la0605844
20. Ye J, Dorpe PV, Lagae L, Maes G, Borghs G (2009) Observation of plasmonic dipolar anti-bonding mode in silver nanoring structures. Nanotechnology 20(46):465203. doi:10.1088/0957-4484/20/46/465203
21. Aizpurua J, Hanarp P, Sutherland DS, Kall M, Bryant GW, de Abajo FJG (2003) Optical properties of gold nanorings. Phys Rev Lett 90(5):057401. doi:10.1103/PhysRevLett.90.057401
22. Halpern AR, Corn RM (2013) Lithographically patterned electrodeposition of gold, silver, and nickel nanoring arrays with widely tunable near-infrared plasmonic resonances. Acs Nano 7(2):1755–1762. doi:10.1021/nn3058505
23. Turkevich J, Stevenson PC, Hillier J (1951) A study of the nucleation and growth processes in the synthesis of colloidal gold. Discuss Faraday Soc 11:55–75. doi:10.1039/df9511100055
24. Chen Y, Nguyen A, Niu L, Corn RM (2009) Fabrication of DNA microarrays with poly(L-glutamic acid) monolayers on gold substrates for SPR imaging measurements. Langmuir 25(9):5054–5060. doi:10.1021/la804021t
25. Kedenburg S, Vieweg M, Gissibl T, Giessen H (2012) Linear refractive index and absorption measurements of nonlinear optical liquids in the visible and near-infrared spectral region. Opt Mater Express 2(11):1588–1611. doi:10.1364/ome.2.001588
26. Kubo W, Fujikawa S (2011) Au double nanopillars with nanogap for plasmonic sensor. Nano Lett 11(1):8–15. doi:10.1021/nl100787b
27. Verellen N, Van Dorpe P, Huang C, Lodewijks K, Vandenbosch GAE, Lagae L, Moshchalkov VV (2011) Plasmon line shaping using nanocrosses for high sensitivity localized surface plasmon resonance sensing. Nano Lett 11(2):391–397. doi:10.1021/nl102991v
28. Lee H, Dellatore SM, Miller WM, Messersmith PB (2007) Mussel-inspired surface chemistry for multifunctional coatings. Science 318(5849):426–430. doi:10.1126/science.1147241
29. Lynge ME, van der Westen R, Postma A, Stadler B (2011) Polydopamine-a nature-inspired polymer coating for biomedical science. Nanoscale 3(12):4916–4928. doi:10.1039/c1nr10969c
30. Wood JB, Szyndler MW, Halpern AR, Cho K, Corn RM (2013) Fabrication of DNA microarrays on polydopamine-modified gold thin films for SPR imaging measurements. Langmuir 29(34):10868–10873. doi:10.1021/la402425n
31. Sendroiu IE, Gifford LK, Luptak A, Corn RM (2011) Ultrasensitive DNA microarray biosensing via in situ RNA transcription-based amplification and nanoparticle-enhanced SPR imaging. J Am Chem Soc 133(12):4271–4273. doi:10.1021/ja2005576
32. Chen C-Y, Un I-W, Tai N-H, Yen T-J (2009) Asymmetric coupling between subradiant and superradiant plasmonic resonances and its enhanced sensing performance. Opt Express 17(17):15372–15380. doi:10.1364/oe.17.015372
33. Shen Y, Zhou J, Liu T, Tao Y, Jiang R, Liu M, Xiao G, Zhu J, Zhou Z-K, Wang X, Jin C, Wang J (2013) Plasmonic gold mushroom arrays with refractive index sensing figures of merit approaching the theoretical limit. Nat Commun. doi:10.1038/ncomms3381